Geomagnetically trapped, albedo and solar particles: trajectory analysis and flux reconstruction with PAMELA

Alessandro Bruno
Bari University and INFN, Italy

on behalf of the PAMELA collaboration

Solar Energetic Particles (SEP), Solar Modulation and Space Radiation: New Opportunities in the AMS-02 Era
Honolulu, Hawai'i, October 18-23, 2015

Outline

- Introduction
- Geomagnetically trapped particles
- Albedo particles
- Geomagnetic cutoff variations
- Solar energetic particles
- Conclusions

PAMELA measurements at low Earth's orbits

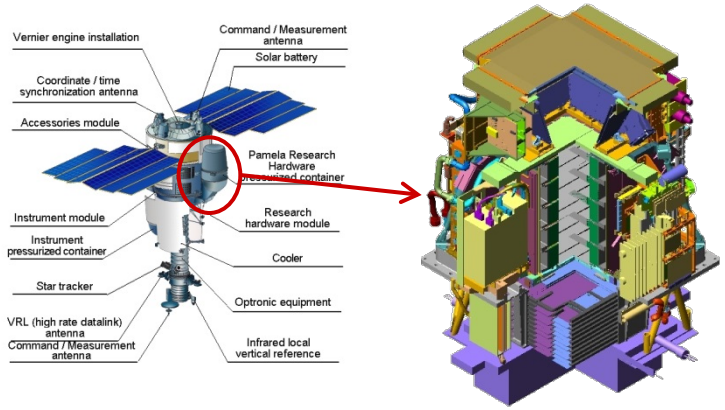

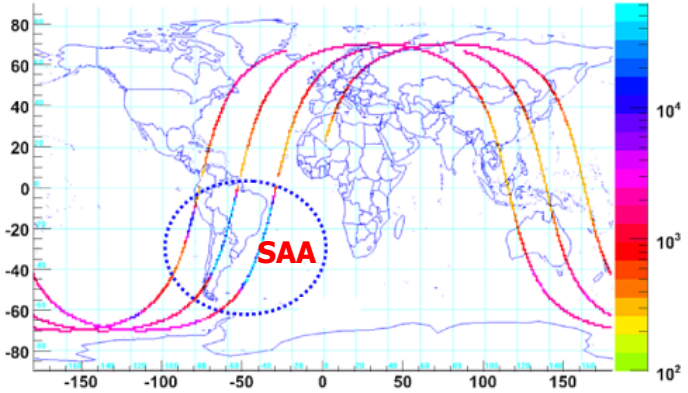

- precise rigidity measurements
  - wide range
- sensitive to composition
  - p/pbar, e+/e-, light nuclei
- semi-polar (70 deg) and elliptic (350 - 610 km) orbit
  - polar caps (low energy CRs & SEPs)
  - geomagnetically trapped (SAA) and albedo
- good angular resolution (~2 deg)
  - possibility to investigate flux anisotropies

PAMELA data analysis
and trajectory reconstruction

PAMELA data:
- spacecraft position & orientation
- particle rigidity and direction
(provided by the tracking system)

IMF, SW and geomagnetic parameters:
- high-resolution (5-min) OMNIWeb data
NASA/Goddard Space Flight Center

NB: the magnetospheric configuration is **updated event by event**, intepolating involved parameters

TRAJECTORY TRACING CODE

Runge-Kutta integration of motion equations
- Based on Smart & Shea (2000, 2005)

Realistic description of the geomagnetic field:
- internal sources: **IGRF11**
- external sources: **TS05/TS07D**

Trajectories propagated back and forth from the measurement location with no limit on tracing time/path

Interplanetary (SCR+GCR)
- (back-traced) trajectories escape the model magnetosphere

Albedo
- (back-traced) trajectories intersect the atmosphere (40km)

Geomagnetically trapped
- trajectories perform more than ~$10^6/R^2$ steps for both propagation directions (≥4 drift cycles)

NB: step-length ~1% of particle gyro-distance in the magnetic field

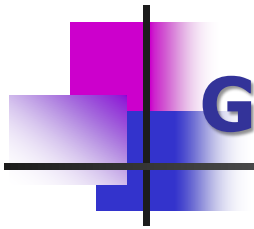

Geomagnetically trapped protons

Data analysis
Adiabatic invariants

Data analyzed in the frame of **adiabatic theory** of particle motion in the geomagnetic field

Gyro motion:

- V x B acceleration leads to gyro motion about field lines
- frequencies ~kHz
- associated 1st invariant μ, relativistic magnetic moment:

$$\mu = \frac{p^2 \sin^2 \alpha}{2 m_0 B}$$

pitch angle α: $\tan \alpha = \frac{V_\perp}{V_\parallel}$

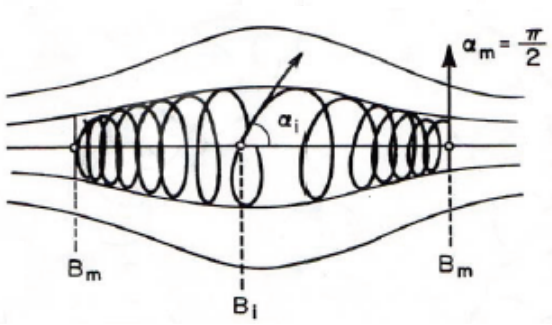

Bounce motion:

- As a particle gyrates down field line, the pitch angle increases as B increases
- Motion along field line reverses when pitch angle reaches 90° (mirror point)
- period ~sec
- associated 2nd invariant K longitudinal invariant:

$$K = \int_{-l_m}^{+l_m} p_\parallel dl$$

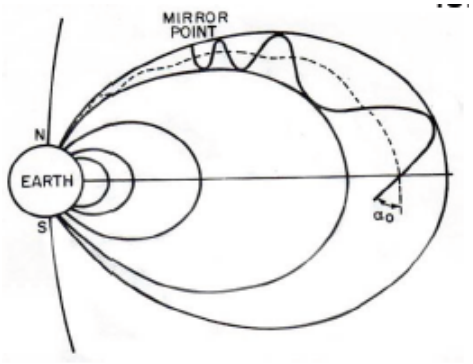

Drift motion:

- Gradient in magnetic field leads to drift motion around Earth: east for electrons, west for protons/ions
- period ~minutes
- associated 3rd invariant ϕ, magnetic flux:

$$\Phi = -\frac{2\pi B_E R_E^2}{L}$$

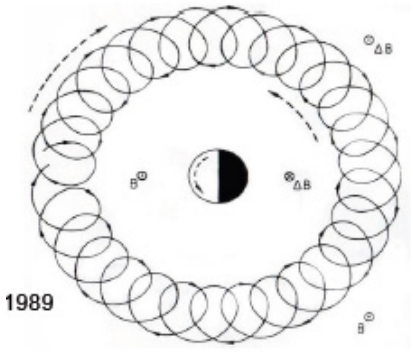

Flux calculation
Differential directional fluxes

- Flux intensities are properly estimated accounting for the flux anisotropic distribution (SAA)

- At former stage, proton fluxes are evaluated as a function of geographic position **X**=(Lon, Lat, Alt) and particle rigidity **R** and α pitch-angle with respect to the geomagnetic field:

proton counts corrected by selection efficiencies

$$F\left(\hat{X},R,\alpha\right)=\frac{N\left(\hat{X},R,\alpha\right)}{2\pi\sum_{\Psi\to\hat{X}}\left[H\left(\Psi,R,\alpha\right)\cdot\Delta T\left(\Psi\right)\right]\cdot\Delta R}$$

sum over satellite orientations Ψ at geographic position **X**

livetime spent by PAMELA at each spacecraft orientation Ψ

PAMELA's effective area

$$H\left(R,\alpha\right)=\frac{\sin\alpha}{2\pi}\int_0^{2\pi}d\beta\left[A\left(R,\vartheta,\varphi\right)\cos\vartheta\right]$$

evaluated with MC methods

apparatus response function

- The relationship between local (ϑ,φ - PAMELA frame) and magnetic (α,β) angles describing particle direction, depends on the satellite orientation Ψ with respect to the geomagnetic field.
- PAMELA's effective area is rigidity dependent due to the bending effect of the magnetic spectrometer.
- No assumption on α distribution is done (e.g. by using sampling fuctions such as $\sin^n\alpha$)

Flux calculation
Differential directional fluxes

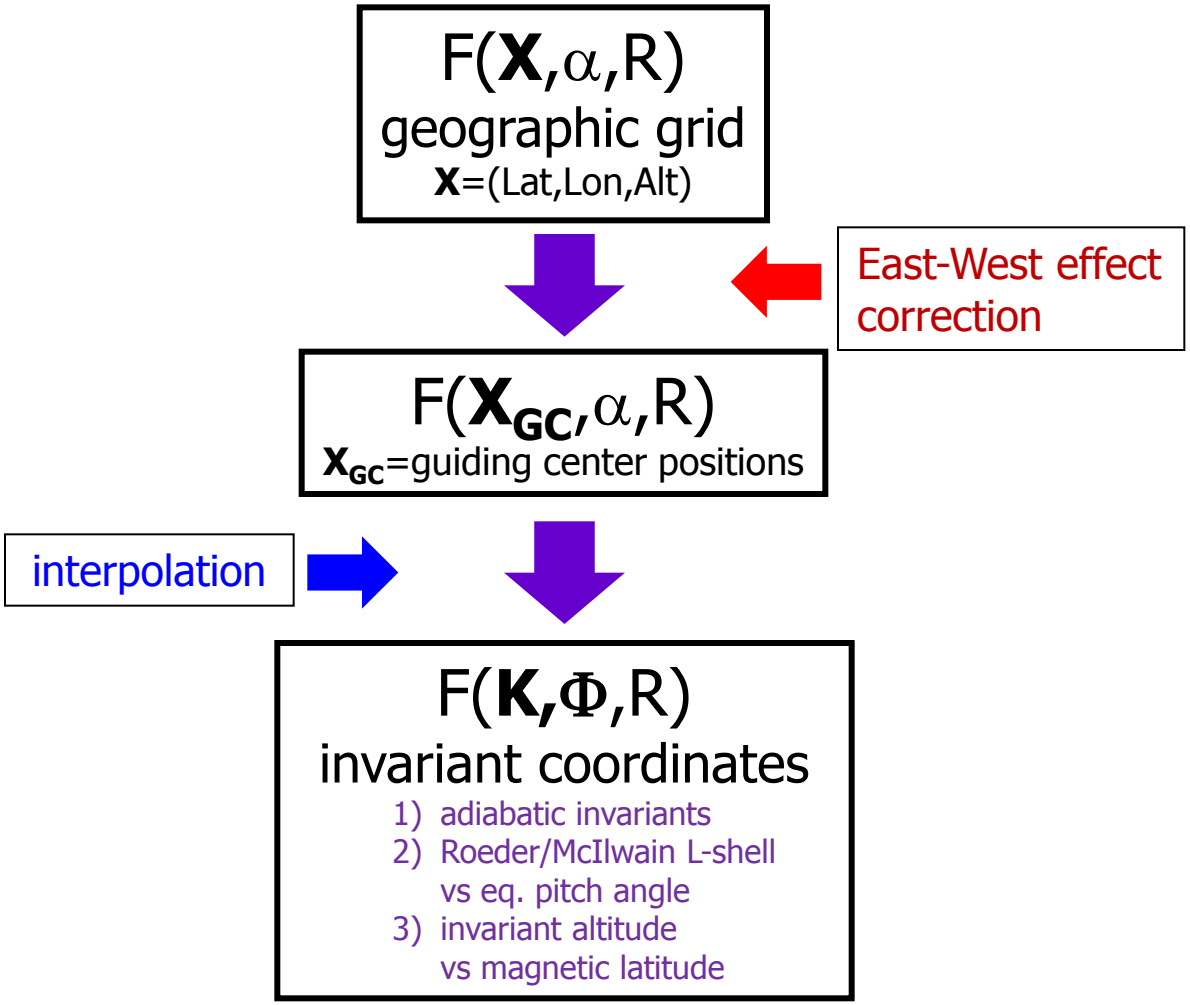

Flux results
Geographic Maps

columns: same energy bins
rows: same altitude bins

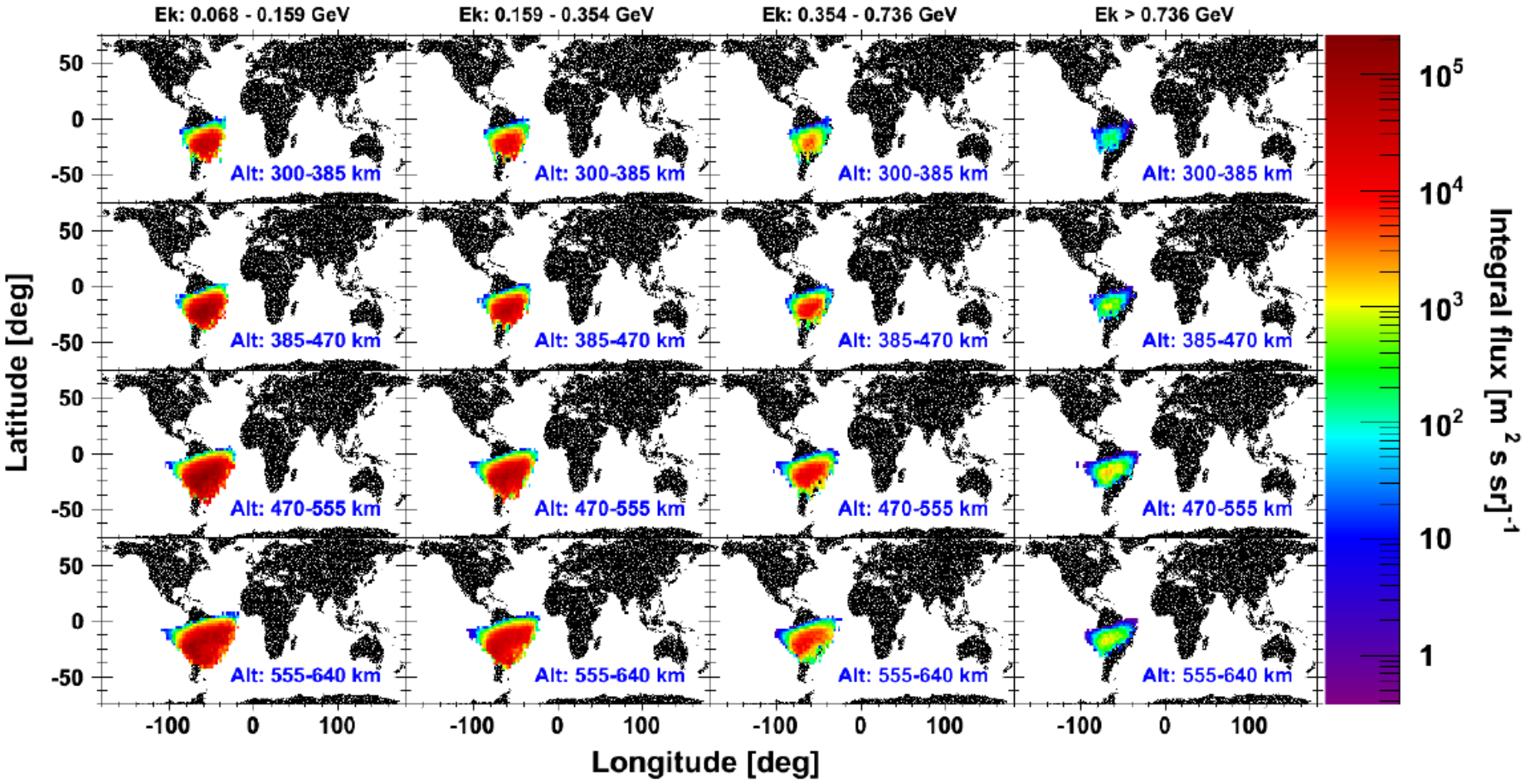

Stably-trapped integral flux ($m^{-2}s^{-1}sr^{-1}$) averaged over the pitch angle range covered by PAMELA, as a function of geographic coordinates, evaluated for different energy (columns) and guiding center altitude (rows) bins.

Adriani et al., 2015, ApJ 799 L4

Flux results
Adiabatic invariants

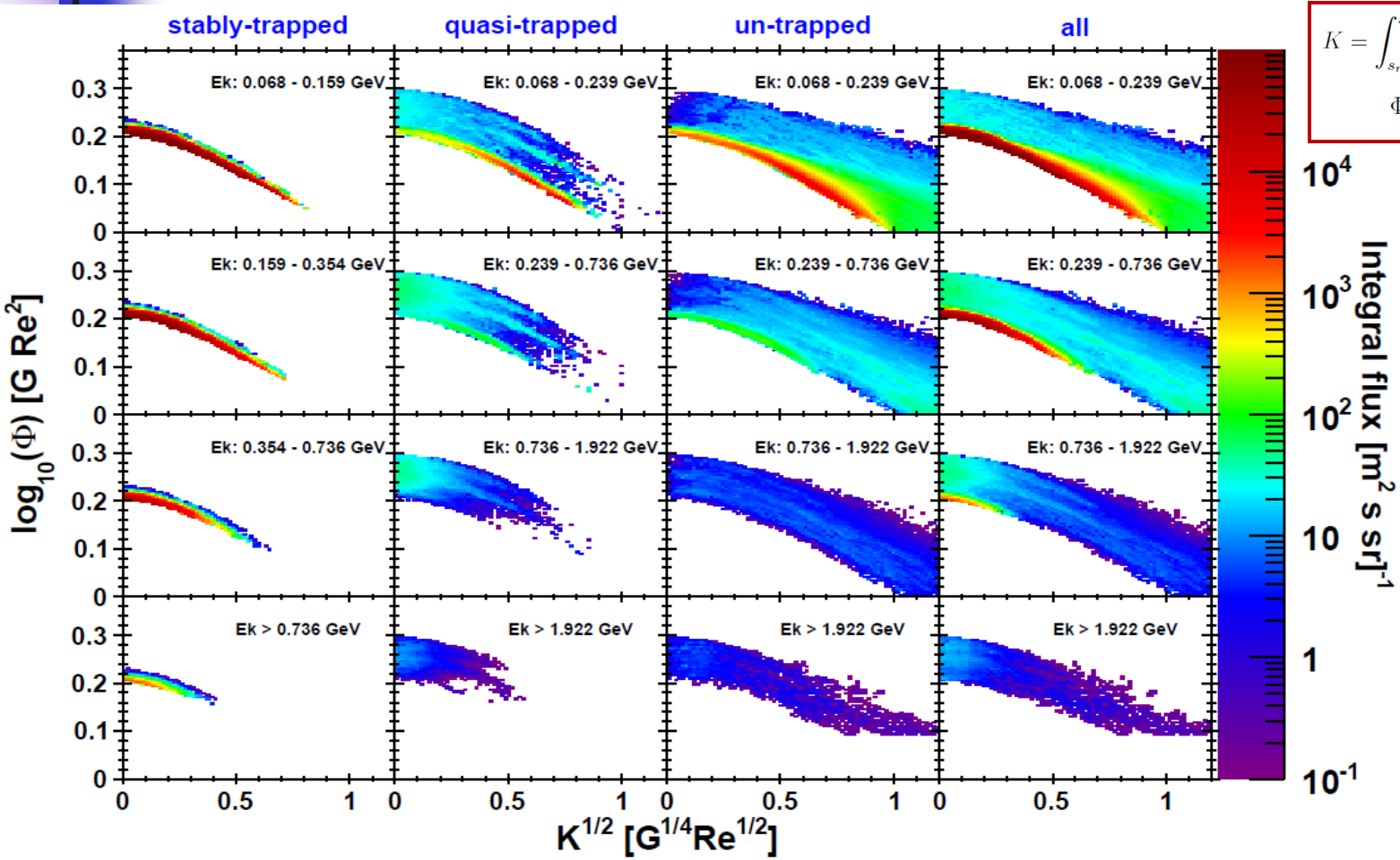

$$K = \int_{s_m}^{s'_m} [B_m - B(s)]^{1/2} ds$$

$$\Phi = \oint \mathbf{A} \cdot \mathrm{dl}$$

Proton integral fluxes ($m^{-2}s^{-1}sr^{-1}$) as a function of the second *K* and the third Φ adiabatic invariant, for different kinetic energy bins (see the labels).
Results for the different populations are reported (from left to right): stably-trapped, quasi-trapped, un-trapped and the total under-cutoff proton sample.

Adriani et al., 2015, ApJ 799 L4

Flux results

Equatorial pitch angle vs L-shell

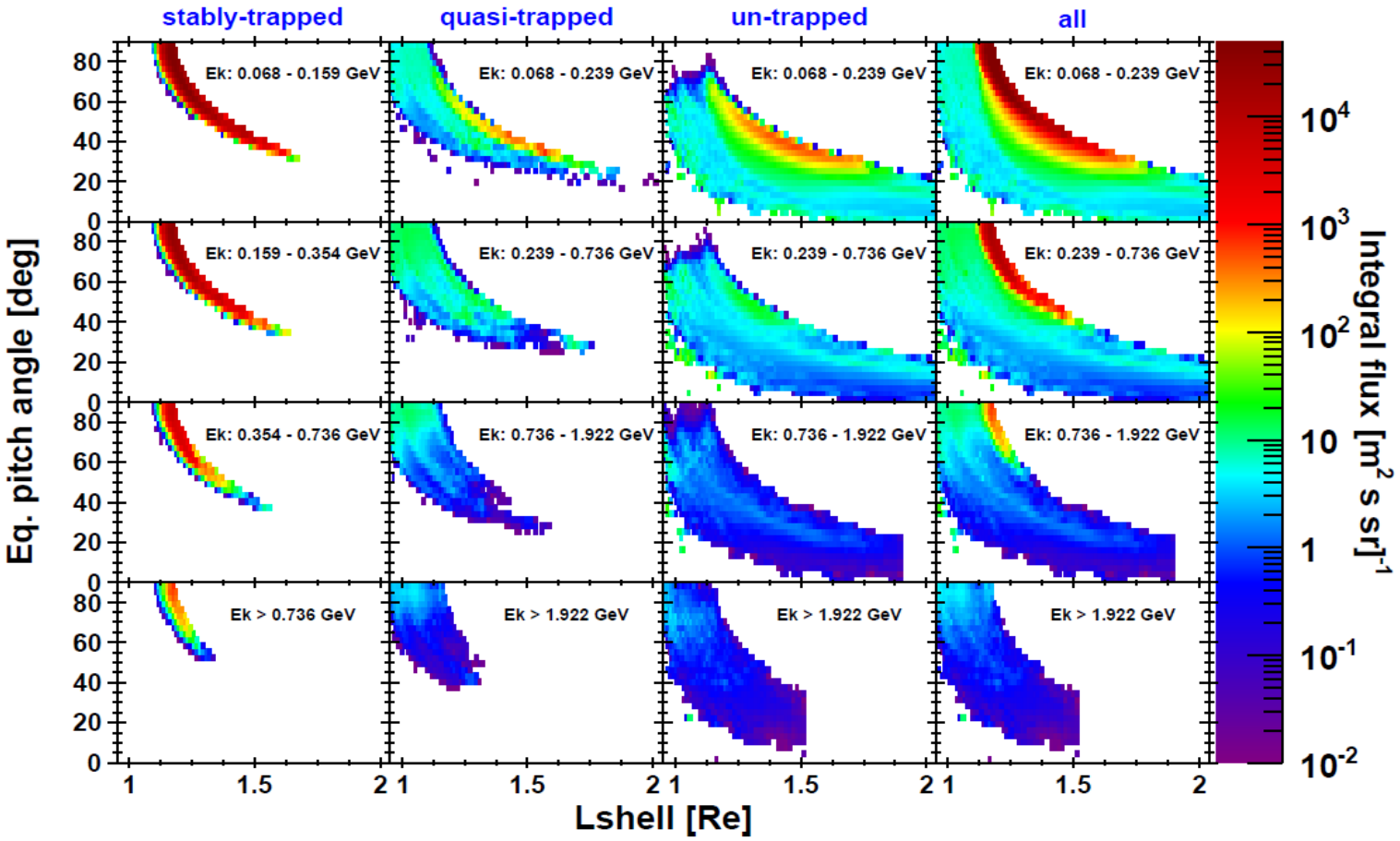

Proton integral fluxes ($m^{-2}s^{-1}sr^{-1}$) as a function of equatorial pitch angle and McIlwain's *L*-shell, for different kinetic energy bins (see the labels).
Results for the different populations are reported (from left to right): stably-trapped, quasi-trapped, un-trapped and the total under-cutoff proton sample.

Adriani et al., 2015, ApJ 799 L4

Trapped fluxes

Comparison with semi-emphirical models

Stably-trapped differential fluxes ($GeV^{-1}m^{-2}s^{-1}sr^{-1}$) compared with predictions from **AP8-min** (Sawyer & Vette 1976) and **PSB97** (Heynderickx et al. 1999) semi-empirical models, denoted with dashed black line and the solid blue line respectively. Model calculations from the SPENVIS on-line system (Heynderickx et al. 2000).

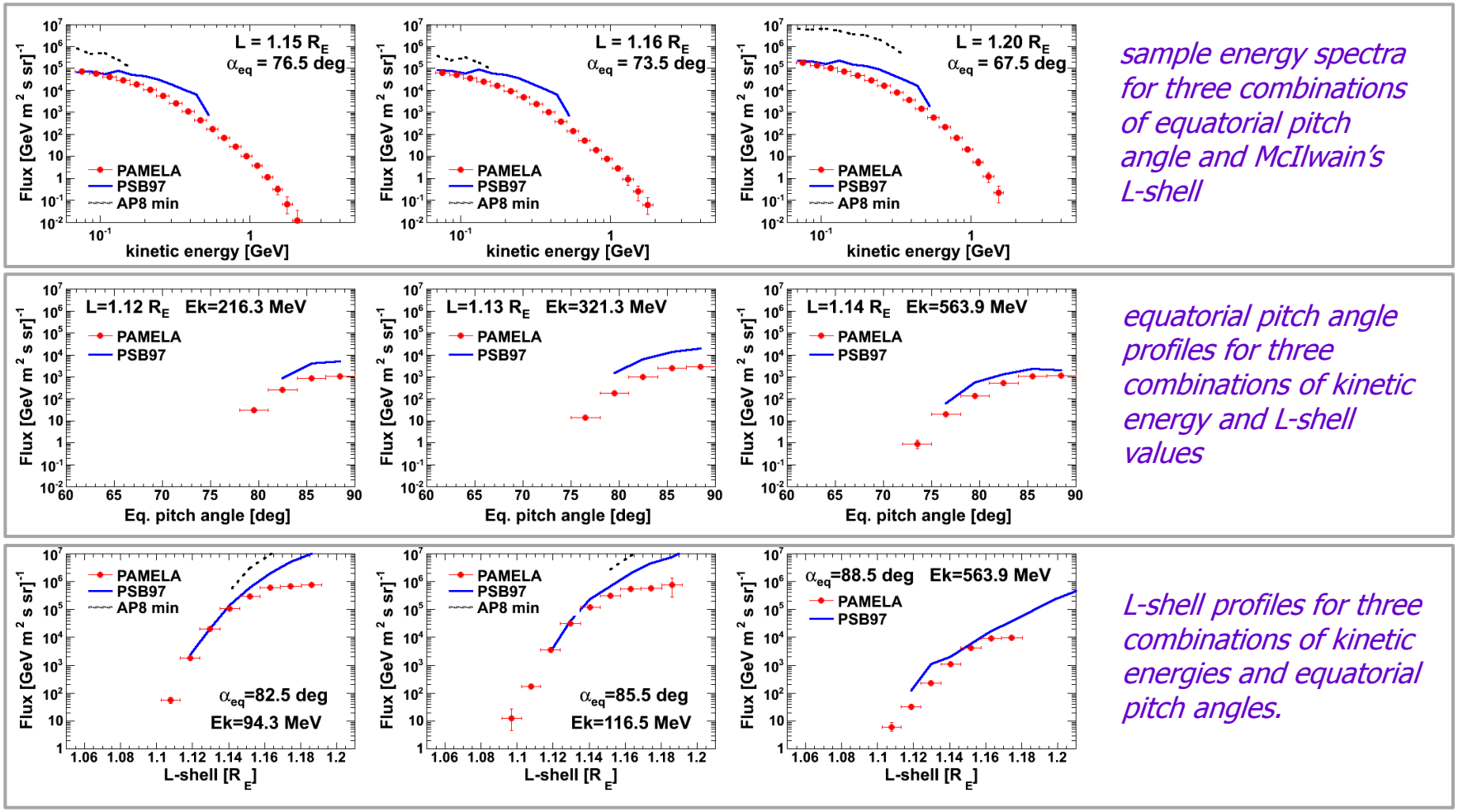

sample energy spectra for three combinations of equatorial pitch angle and McIlwain's L-shell

equatorial pitch angle profiles for three combinations of kinetic energy and L-shell values

L-shell profiles for three combinations of kinetic energies and equatorial pitch angles.

Adriani et al., 2015, ApJ 799 L4

Trapped fluxes
Comparison with theoretical models

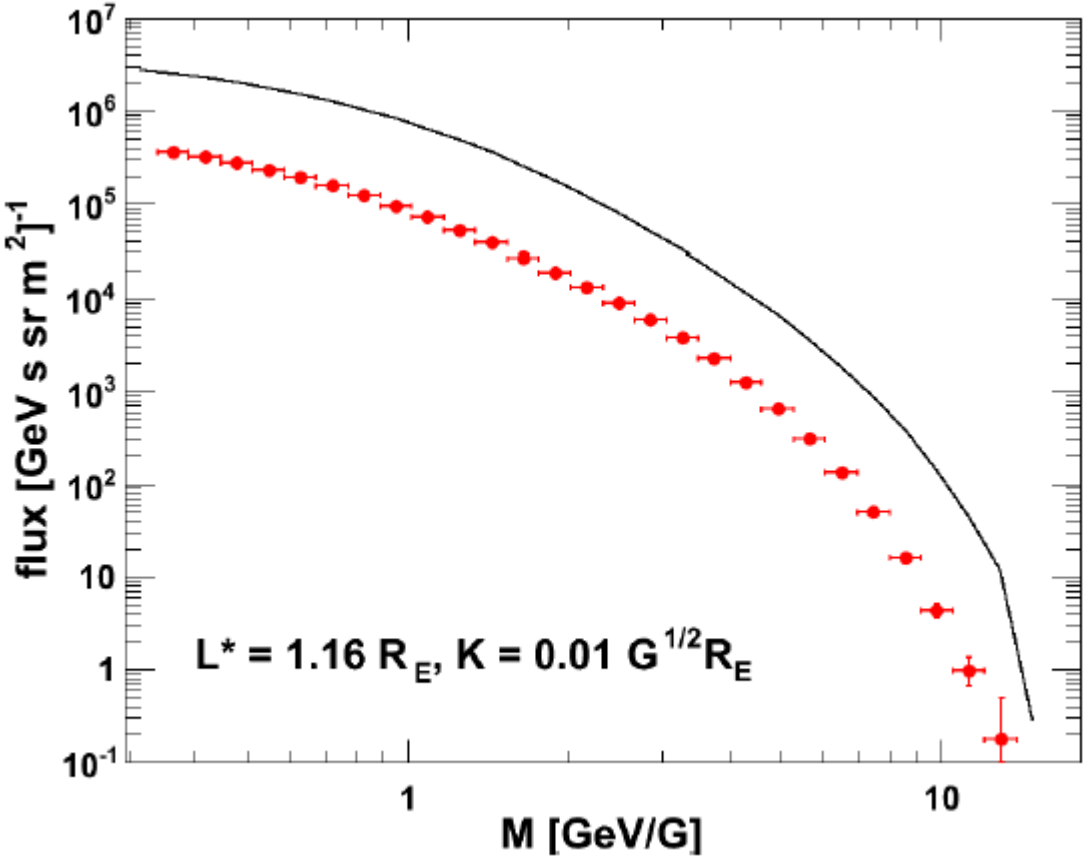

$$L^* = \frac{2\pi\mu_E}{R_E\Phi}$$

Stably-trapped differential flux (GeV^{-1}m^{-2}s^{-1}sr^{-1}) at geomagnetic equator compared with the calculation by **Selesnick et al. (2007)** for the year 2000. Spectra are reported as a function of the 1st adiabatic invariant M, for sample values of K (2nd adiabatic invariant) and L* (Roeder's parameter) invariants.

Adriani et al., 2015, ApJ 799 L4

The discovery of geomagnetically trapped antiprotons

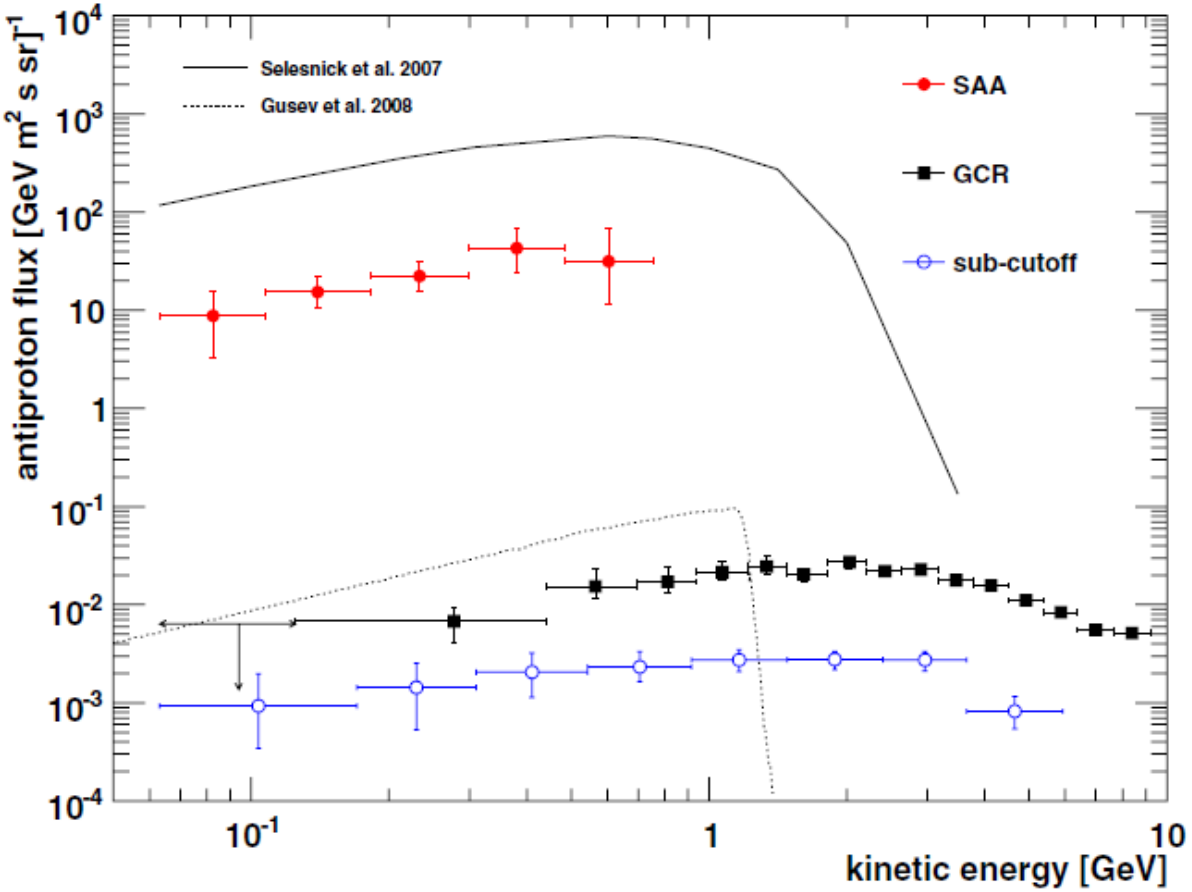

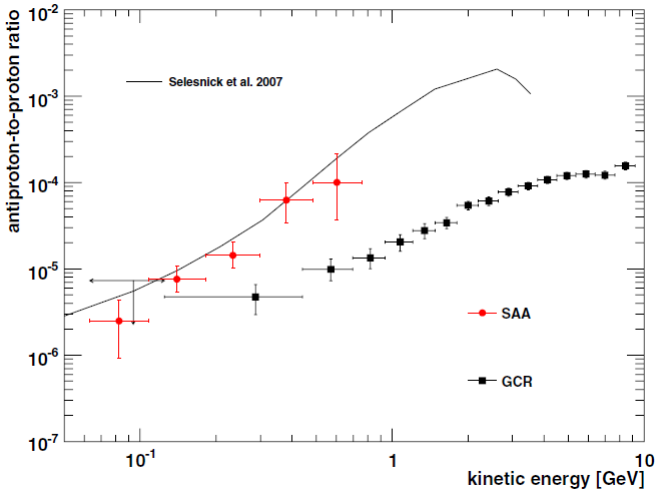

pbar/p ratio in SAA

Adriani et al., ApJL, 2011, 737:L29

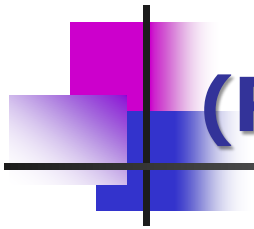

(Re-entrant) albedo protons

Albedo classification

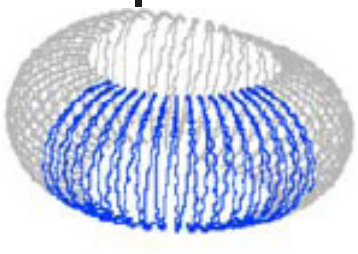

Lifetime = the time between the particle origin (traced backward) and its subsequent absorption (traced forward) in the atmosphere (40 km).

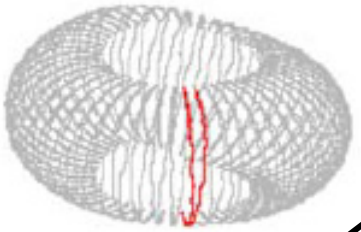

Since the quasi-trapped lifetime is of the order of a half drift period, which scales with $\sim 1/\gamma\beta^2$, lifetime and energy have an approximately inverse proportional relation

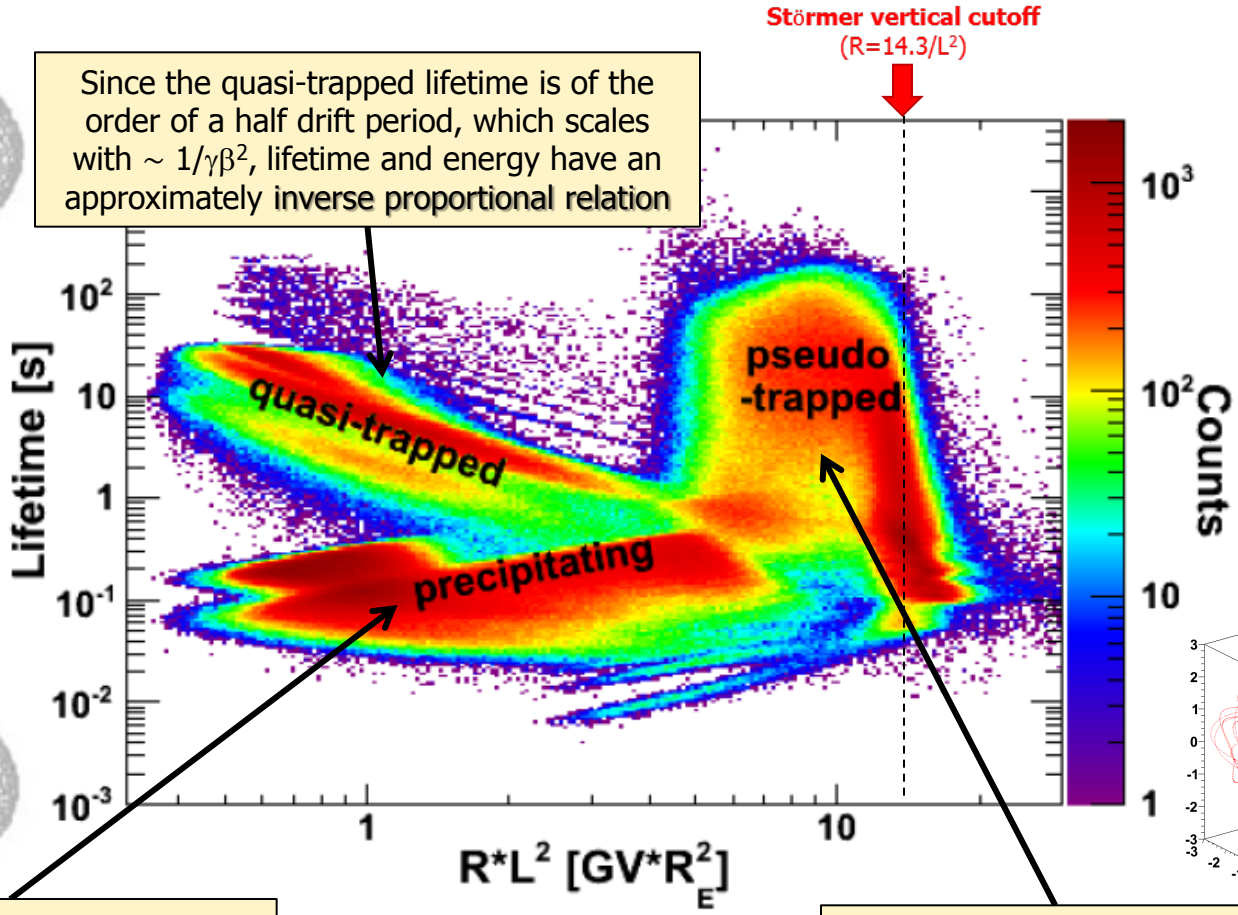

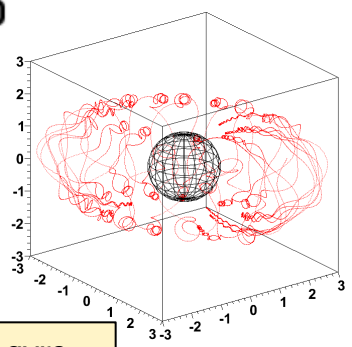

The precipitating lifetime is shorter than the typical bounce period, which scales with $1/\beta$, resulting in a weaker dependency on energy

Non-adiabatic or large gyro-radius effects cause the breakdown of (quasi) trapping conditions: irregular trajectories with no periodicity

Adriani et al., 2015, JGR – Space Physics, 120

Albedo protons
Flux maps

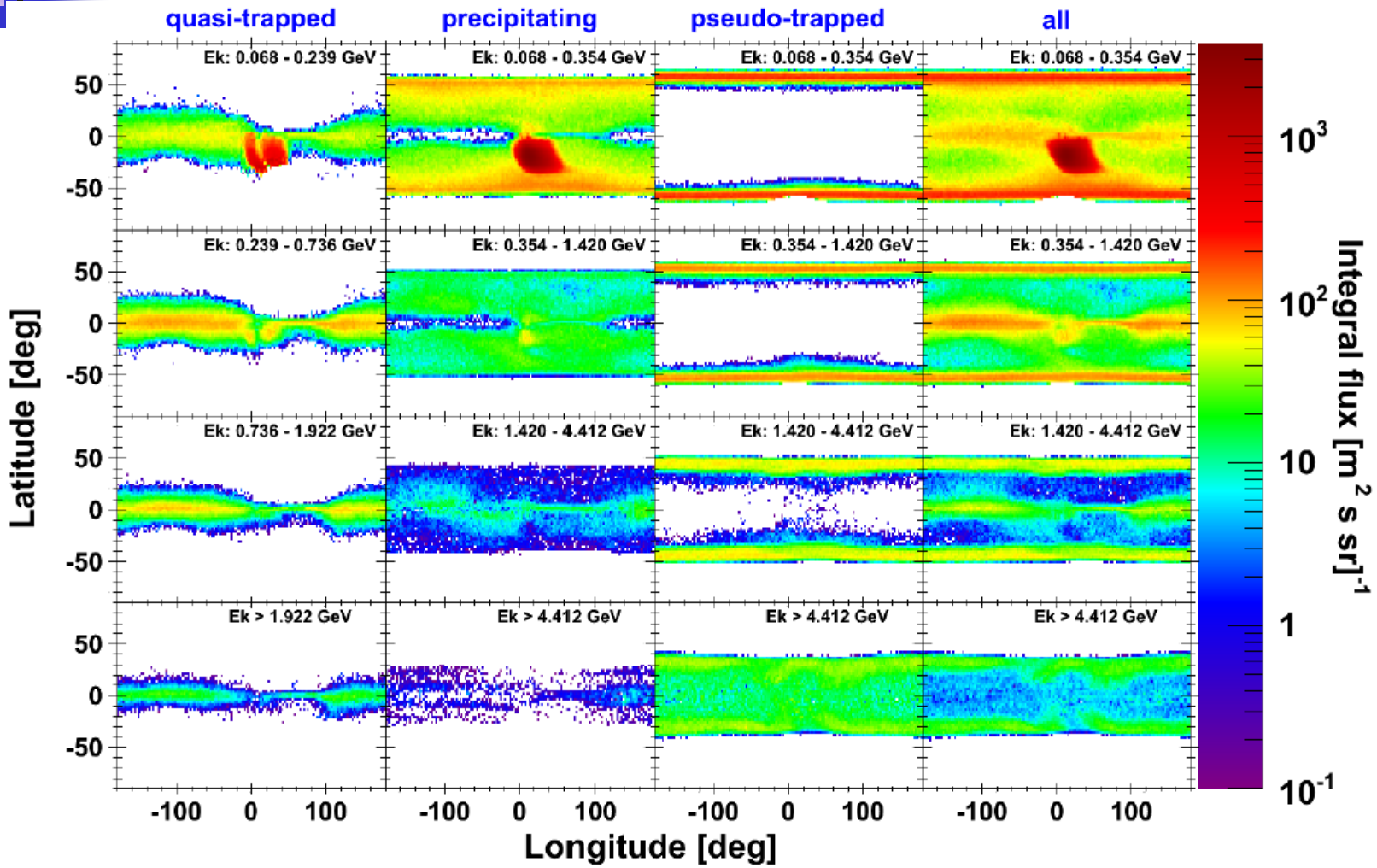

Under-cutoff proton integral fluxes ($m^{-2}s^{-1}sr^{-1}$) as a function of magnetic longitude and latitude, for different energy bins. Results for the several proton populations are reported (from left to right): quasi-trapped, precipitating, un-trapped and the total sample.

Adriani et al., 2015, JGR – Space Physics, 120

Albedo protons

Energy spectra vs latitude

Differential energy spectra outside the SAA region measured for different bins of magnetic latitude (see the labels).

Results for the different proton populations are shown: quasi-trapped (**blue**), precipitating (**green**), pseudo-trapped (**red**) and interplanetary (**black**).

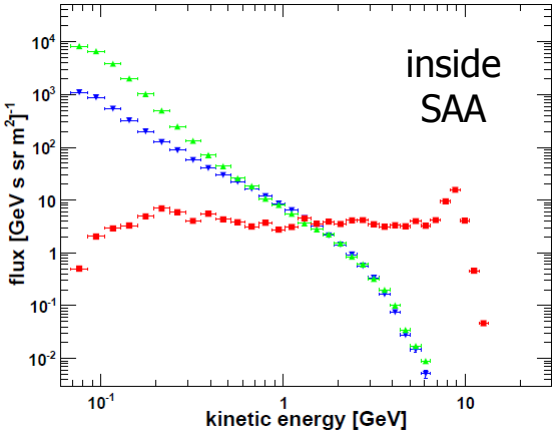

Differential energy spectra in the **SAA** region (B<0.23 G)

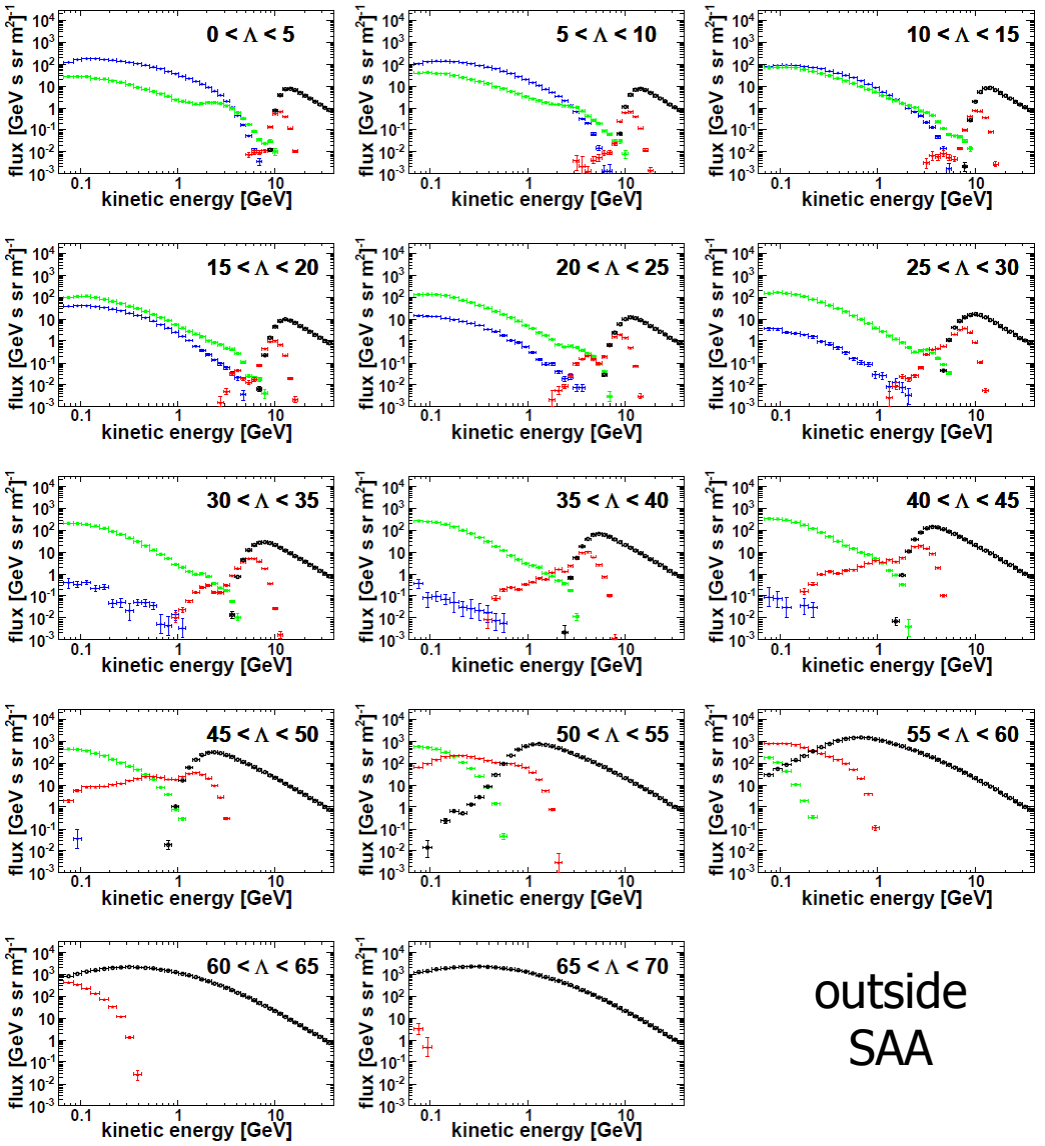

outside SAA

Adriani et al., 2015, JGR – Space Physics, 120

Penumbra region

Penumbra: region where protons of both interplanetary and atmospheric origin are present

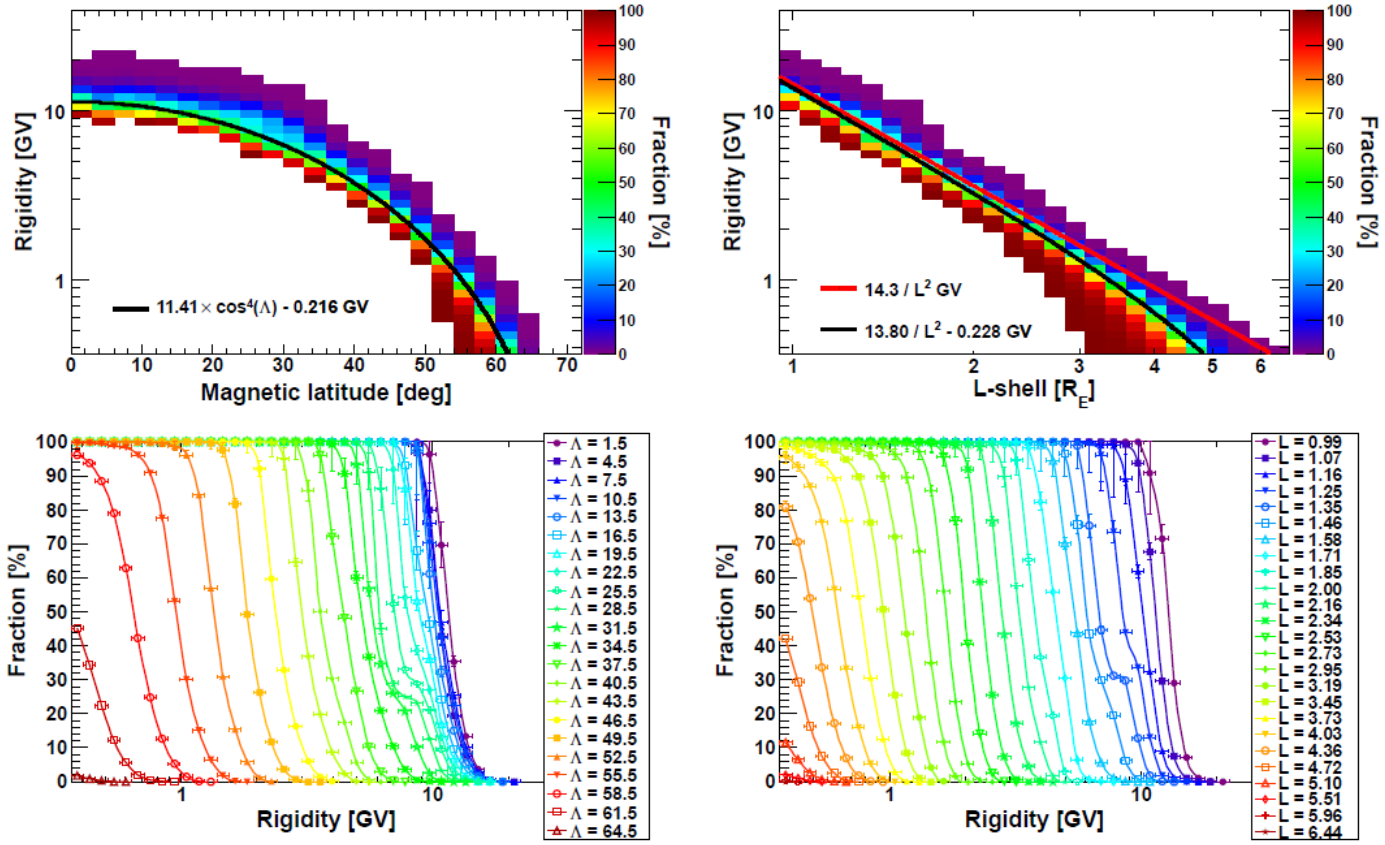

Top panels: fraction of albedo protons in the penumbra region, as a function of particle rigidity and magnetic latitude (left) and McIlwain's *L*-shell (right); black curves are a fit of points with equal percentages of interplanetary and albedo protons, while the red line denotes the Störmer vertical cutoff for the PAMELA epoch.
Bottom panels: corresponding rigidity profiles, for different values of magnetic latitude (left) and McIlwain's *L*-shell (right); values at bin center are reported in labels. Lines are to guide the eye.

Adriani et al., 2015, JGR – Space Physics, 120

Geomagnetic cutoff
Impact of external geomagnetic models

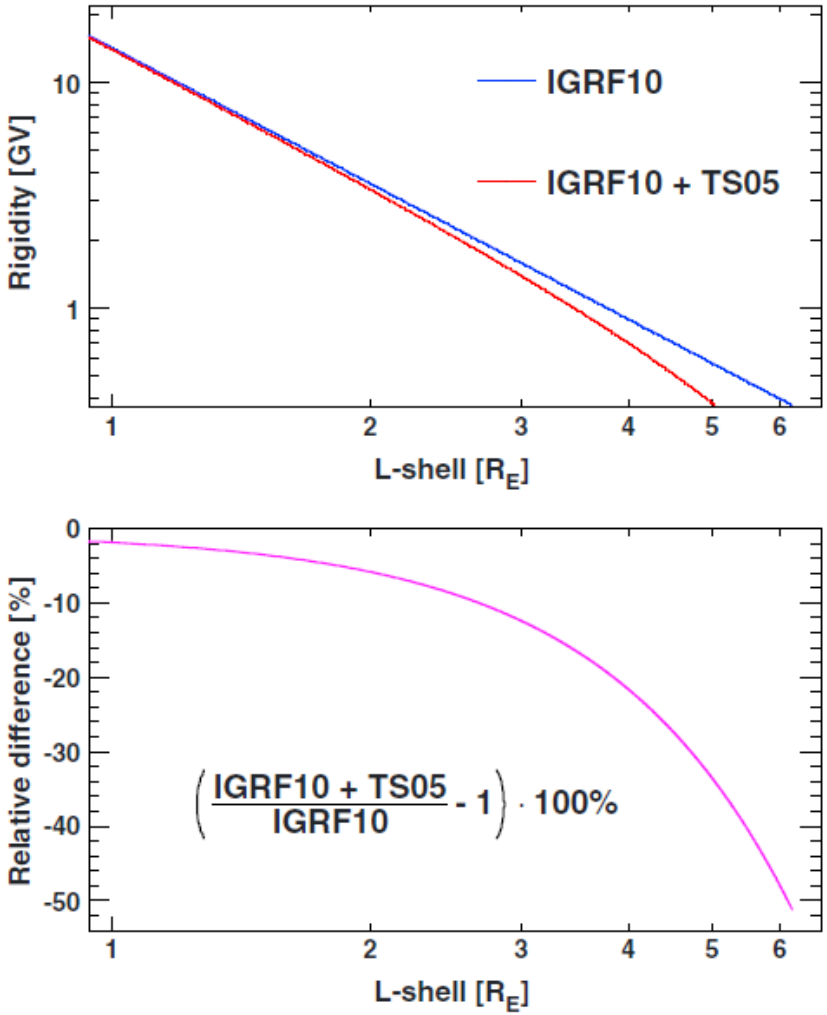

The usage of a realistic external geomagnetic field model has a significant impact on estimates of high-latitude cutoffs.

In case of IGRF standalone, results are in a very good agreement with the standard cutoff relation ($R_{svc}=14.22/L^2$ GV) at all *L*-shells.

On the other hand, significant differences (up to a factor ~2) can be noted between the IGRF10 model and the combined model configuration at highest *L*-shells.

Adriani et al., 2015, JGR – Space Physics, 120

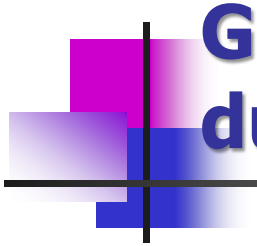

Geomagnetic cutoff variations during SEP events

Evaluation of cutoff latitudes

- The numerical algorithm developed to extract cutoff latitudes from the PAMELA data is similar to one used by *Leske et al.* 2001 and *Kress et al.* 2010:
  - for each rigidity bin, a mean flux was obtained by averaging fluxes above 65 degrees latitude,
  - and the cutoff latitude was evaluated as the latitude where the flux intensity is equal to the **half of the average value**.

- Alternatively, cutoff latitudes were estimated with back-tracing techniques:
  - at a given rigidity, the cutoff latitude was evaluated as the latitude where an **equal percentage** of interplanetary and albedo CRs was registered.

- The calculation was performed for 13 rigidity logarithmic bins, covering the interval 0.39 -- 3.29 GV.

- Accounting for the limited statistics at highest rigidities, final cutoff values were derived by fitting averaged PAMELA observations over **single orbital periods** (94 min).

Bruno et al., PoS(ICRC2015)287

The 2006 Dec 13-14 SEP events

- On 2006 December 13 at 02:14 UT, an **X3.4/4B solar flare** occurred in the active region NOAA 10930 (S06W23; NOAA-STP 2006).
  - This event also produced a full-halo **CME** with a speed of 1774 km s-1.
  - The forward shock of the CME reached Earth at about 14:10 UT on December 14, causing a **Forbush decrease** of Galactic CR intensities that lasted for several days.

- The **flare X1.5** (S06W46) at 21:07 UT on December 14 gave start to a new growth of particle intensity as recorded by PAMELA and other satellites.
  - The maximum energy of protons was below 1 GeV, and therefore no ground level enhancement (GLE) was recorded.
  - The corresponding CME had a velocity of 1042 km s-1.

The December 14-15, 2006 geomagnetic storm
IMF and SW variations

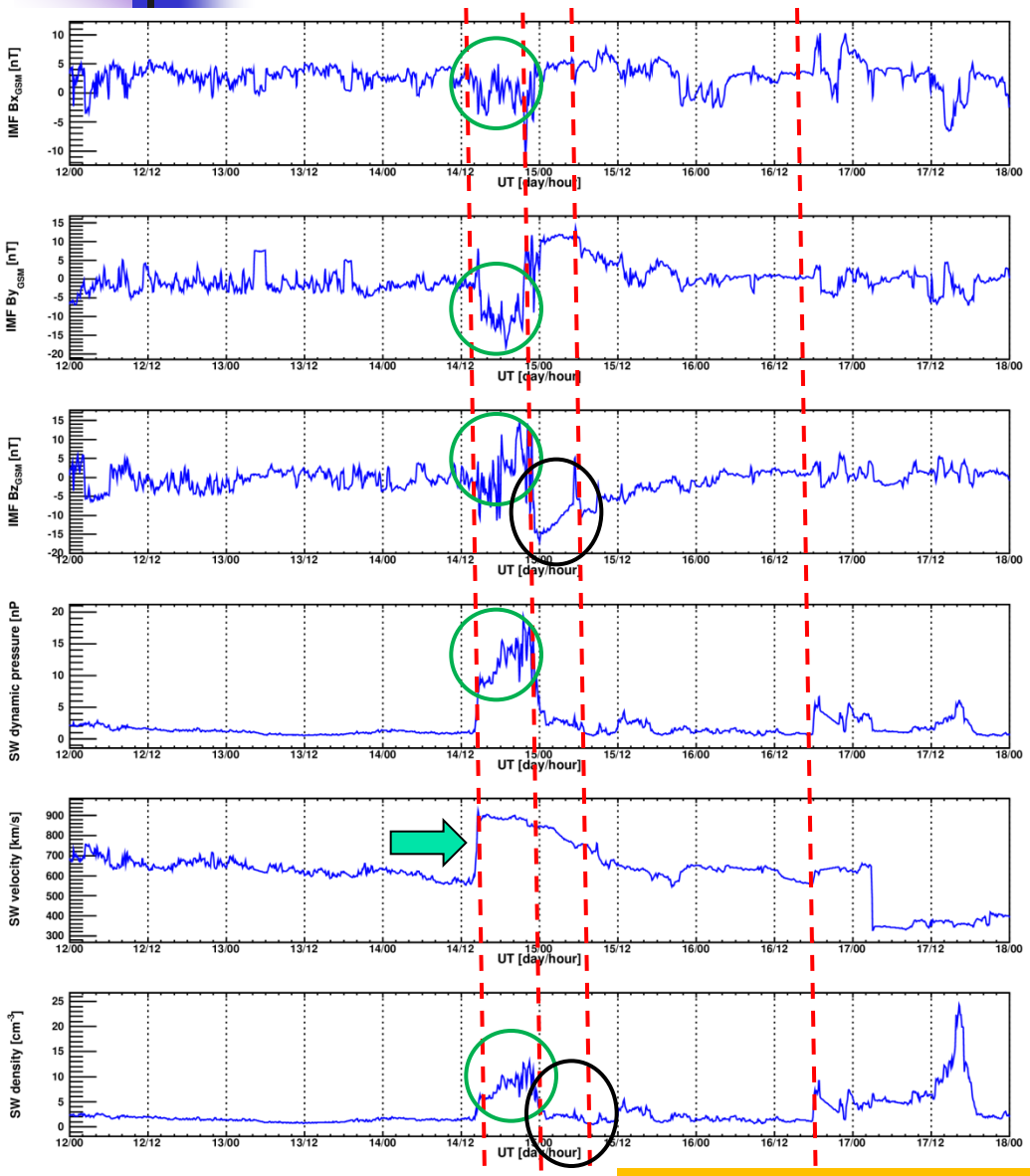

- The large increase in the SW velocity associated with the leading edge of the CME caused the **sudden commencement** of a geomagnetic storm.
- The **initial phase** of the storm, lasting up to about 23:00 UT, was characterized by intense fluctuations in the SW density and in all IMF components.
- At a later stage, the IMF Bz component became negative, the SW density decreased, and the **main phase** of the storm started, reaching a maximum between 02:00--08:00 UT on Dec 15.
- Another interplanetary shock associated with a different CME was observed on December 16.

Bruno et al., PoS(ICRC2015)287

Measured cutoff latitudes

Data missing from 10:00 UT on Dec 13 until 09:14 UT on Dec 14 because of an onboard system reset of the satellite

Time profile of the geomagnetic cutoff latitudes measured by PAMELA for different rigidity bins

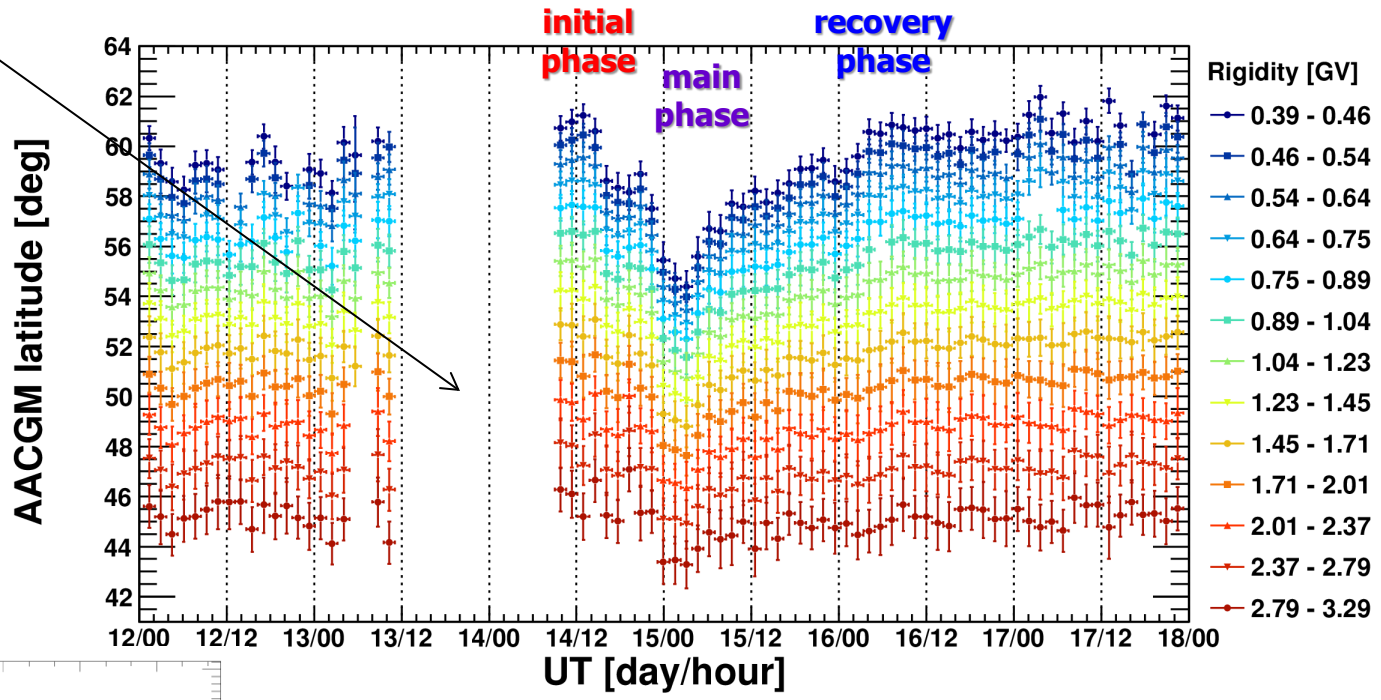

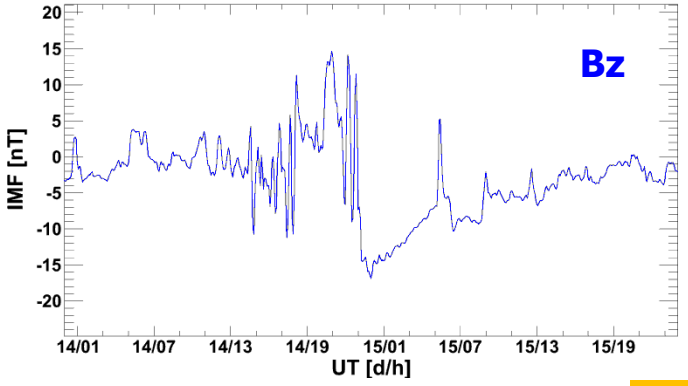

The evolution of the magnetic storm of December 14 and 15 followed the typical scenario in which the cutoff latitudes move equatorward as a consequence of a CME impact on the magnetosphere with an associated transition to southward IMF Bz.

Bruno et al., PoS(ICRC2015)287

Comparison with geomagnetic indexes

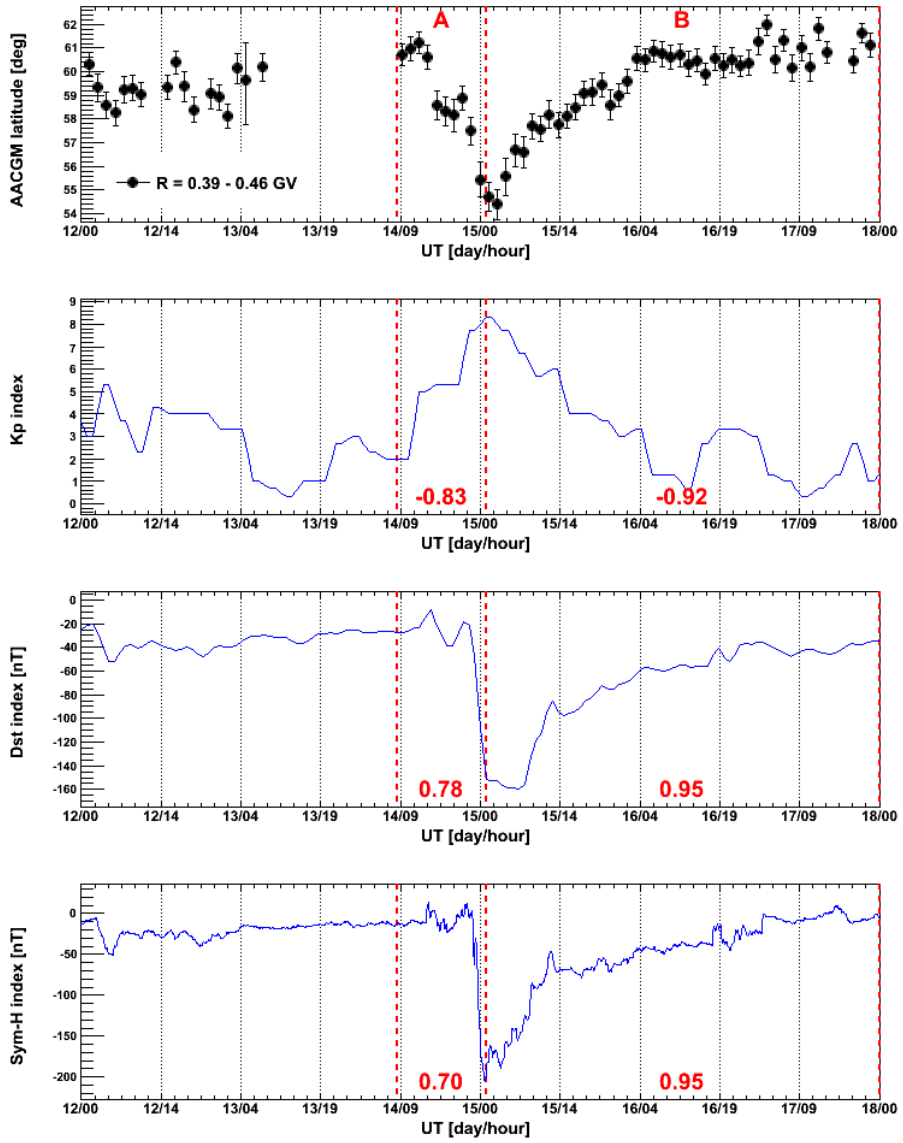

The magnetic activity index (**Kp**), the disturbance storm time index (**Dst**) and the **Sym-H** index,

- measured by ground-based magnetometers,
- at 3-hour, 1-hour, and 1-min resolutions, respectively.

are commonly used to infer cutoff latitudes.

In general, the shapes of the time variations in the cutoff measurements are well correlated with indexes changes

- corresponding correlation coefficients are -0.8, 0.78 and 0.78, respectively.
  - A better agreement is observed for Kp during the initial phase of the storm (A),
  - while the Dst and the Sym-H indexes show an improved correlation during the main and the recovery phases (B).

Bruno et al., PoS(ICRC2015)287

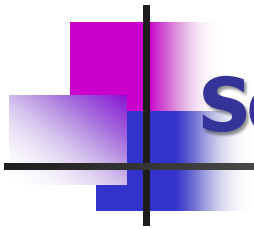

Solar energetic particles (SEPs)

PAMELA SEP's measurements

- wide energy interval: ~80 MeV – several GeV
  - bridging the low energy data by other space-based instruments and the GLE data by the worldwide network of neutron monitors (NMs)
- sensitive to particle composition
  - protons, He nuclei, …
- possibility to reconstruct the angular distribution
  - investigation of flux anisotropies

Trajectory analysis
Motivation

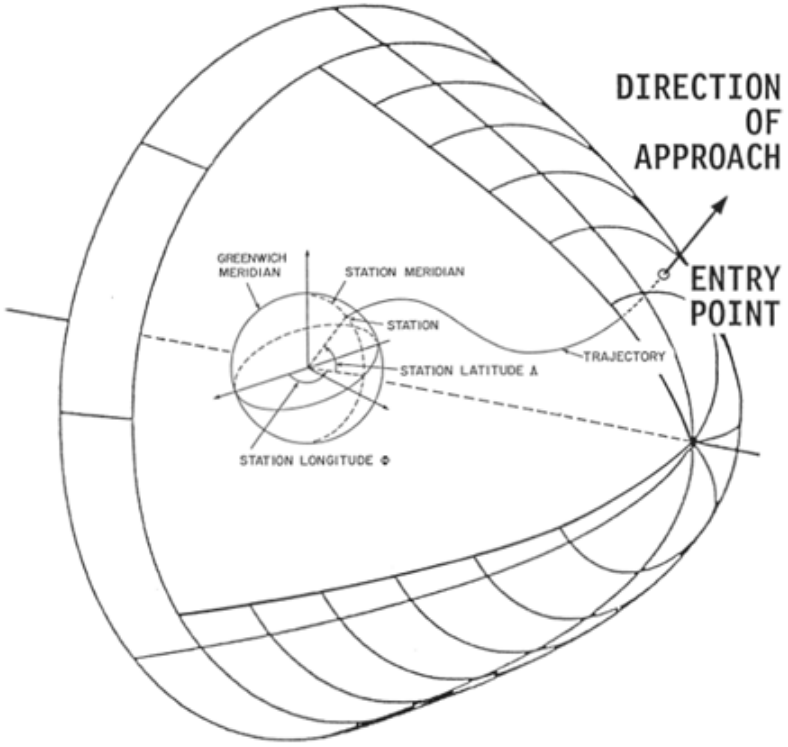

[Shea & Smart, ERP No 524, AFCRL-TR-75-0381, 1975]

- In order to measure SEP angular distributions (and investigate the degree of anisotropy), it is necessary to account for the effect of the geomagnetic field on particle propagation.
- Typically (NMs) one is interested in particle arrival "**asymptotic directions**", i.e. the directions of approach before they enter the magnetosphere.
- To determine asymptotic directions, particle trajectories are reconstructed in a model magnetosphere by means of **numerical integration methods** (Smart & Shea 2005).
- The trajectory analysis also allows to evaluate geomagnetic cutoff rigidities and to separate protons of interplanetary (GCRs & SCRs) and atmospheric (trapped & albedo) origin.

Trajectory analysis
Gemagnetic field models

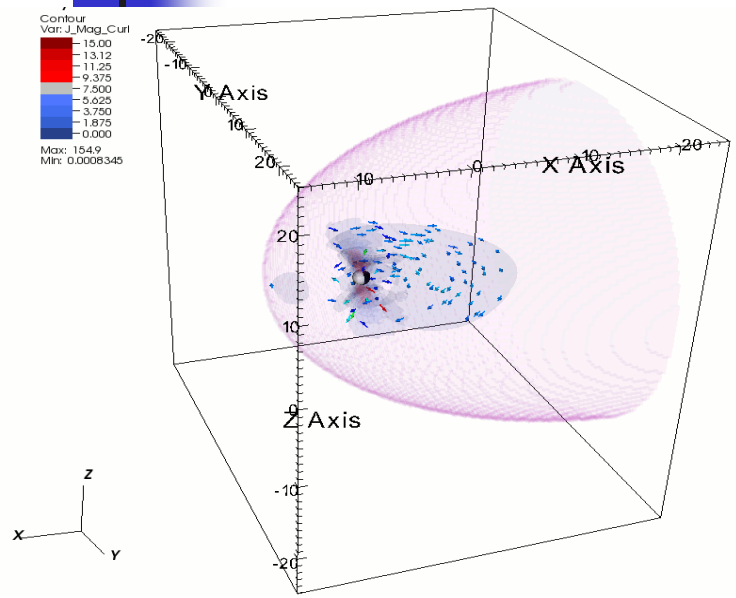

The Tsyganenko models are **semi-empirical** best-fit representations for the external magnetic field

The **TS07D** model (Tsyganenko & Sitnov 2007):

- Dynamical, high-resolution description:
  - large (~10^6 points) dataset based on recent (1995-2005) spacecraft measurements (Cluster, Polar, Geotail, IMP-8, GOES 8-12);
- Coverage: < 30-35 R_E ;
- More flexible and strongly superior to all past empirical models in reconstructing distribution of storm-scale currents.

For more details: http://geomag_field.jhuapl.edu/model/

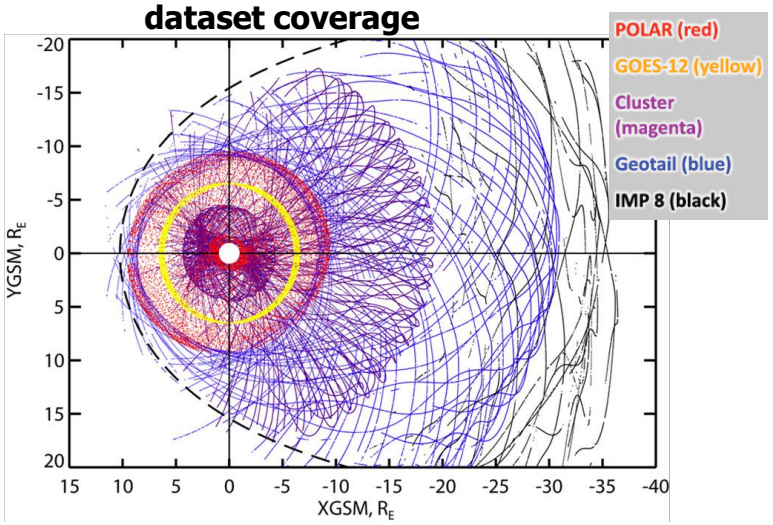

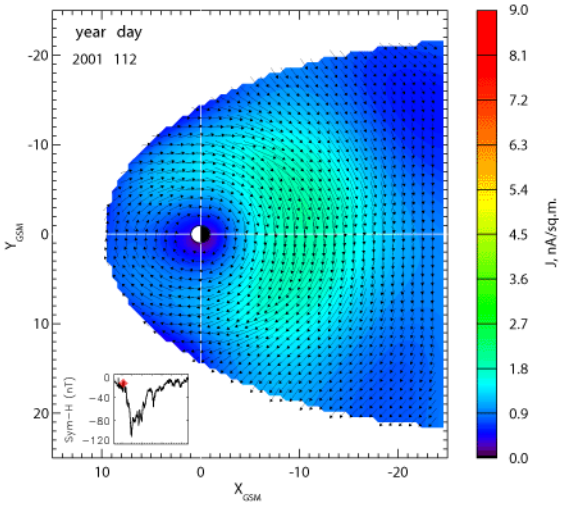

Flux calculation
Effective area calculation

PAMELA effective area:

$$H(R,\alpha) = \frac{\sin\alpha}{2\pi}\int_0^{2\pi} d\beta\left[A(R,\vartheta,\varphi)\cos\vartheta\right]$$

NB: again, no assumption on α distribution (e.g. gaussian)

- The method is similar to the one developed for the estimate of geomagnetically trapped fluxes (as a function of pitch-angle with respect to the local geomagnetic field)

- but in the present case the considered pitch-angle is respect to the IMF (asymptotic)
  - thus not evaluable with simple trigonometric operations
    - at given position/time, the relationship between local and asymptotic angles is rigidity dependent
  - ➢ trajectory analysis is required

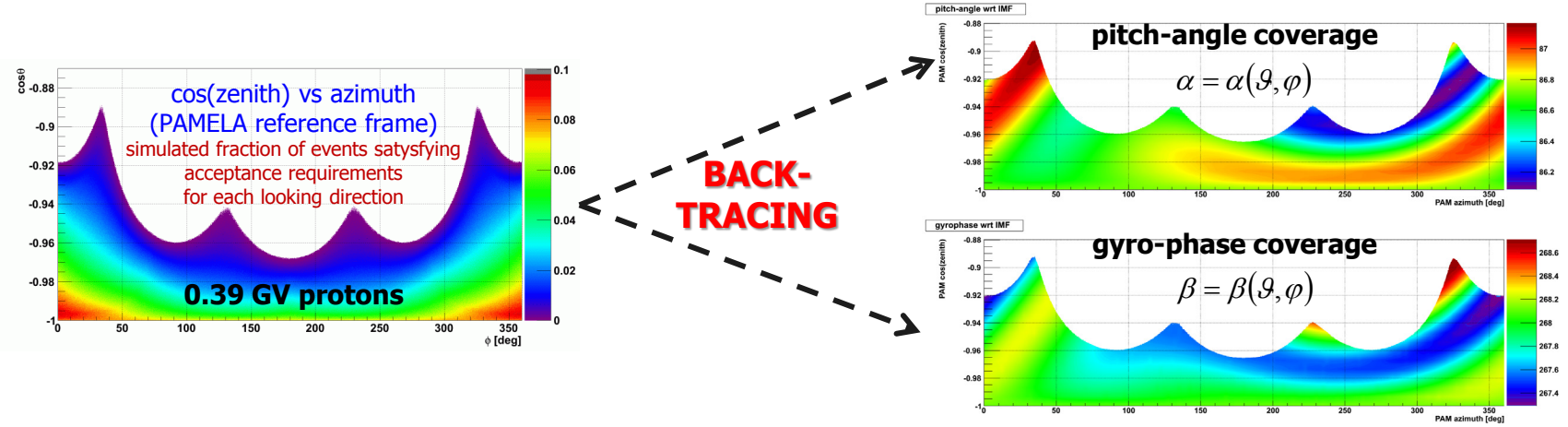

Bruno et al., PoS(ICRC2015)085

Flux calculation
Effective area calculation

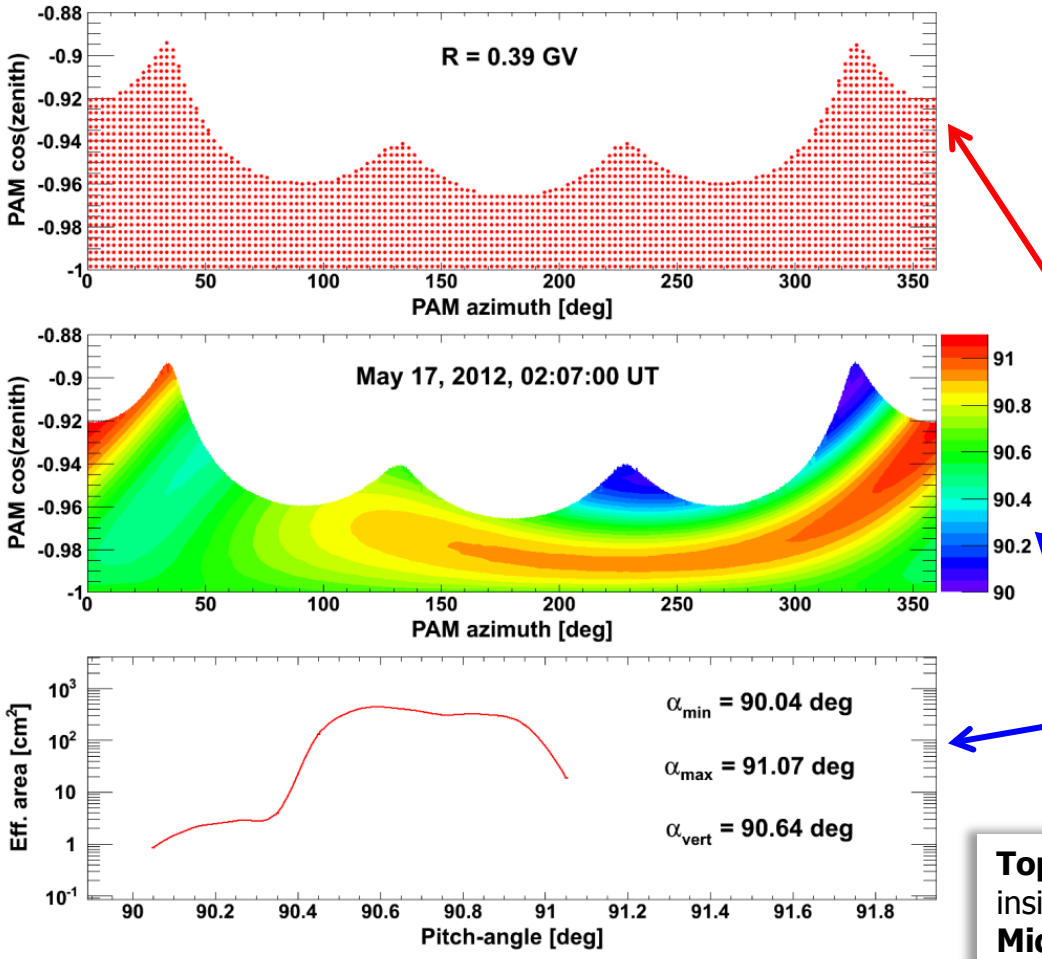

sample orbital position

To convert local into asymptotic directions, a large number of trajectories (uniformly distributed inside PAMELA field of view) has to be reconstructed in the magnetosphere, for each rigidity value and each orbital position.

To assure a **high resolution**, the calculation is performed for time steps with a 1-sec width, by back-tracing about 2800 trajectories, for 22 rigidity bins (0.39 ÷ 4.09 GV)

- more than $8 \cdot 10^7$ trajectories for each polar pass (~23 min)!

At a later stage, results are extended over the full field of view of PAMELA through bilinear interpolation.

Top: distribution of reconstructed directions (red points) inside the PAMELA field of view.
Middle: calculated pitch-angle coverage (color code, deg).
Bottom: the apparatus effective area as function of pitch-angle. Results correspond to 0.39 GV protons, for a sample orbital position (May 17, 2012, 02:07 UT).

Bruno et al., PoS(ICRC2015)085

Flux calculation
Effective area calculation

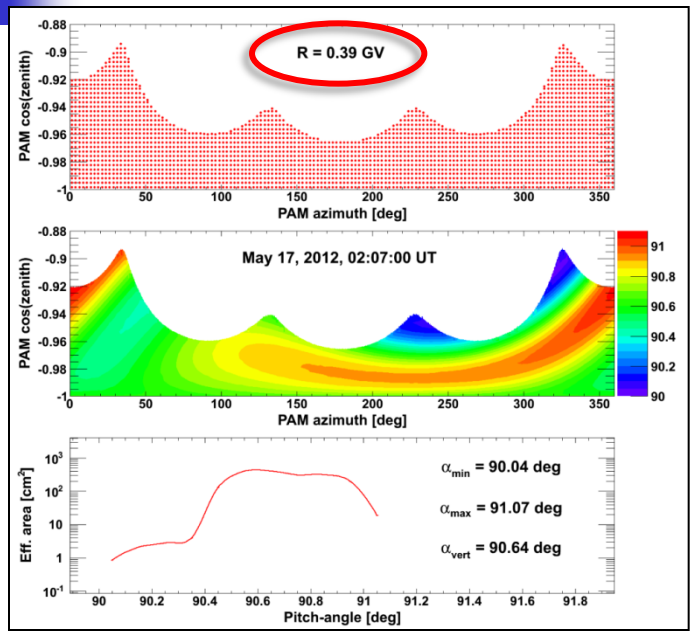

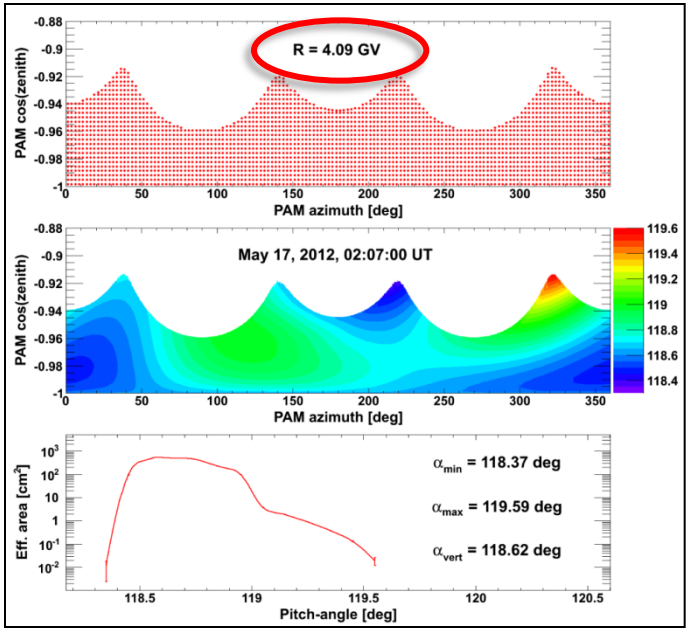

peaks: vertical asymptotic directions

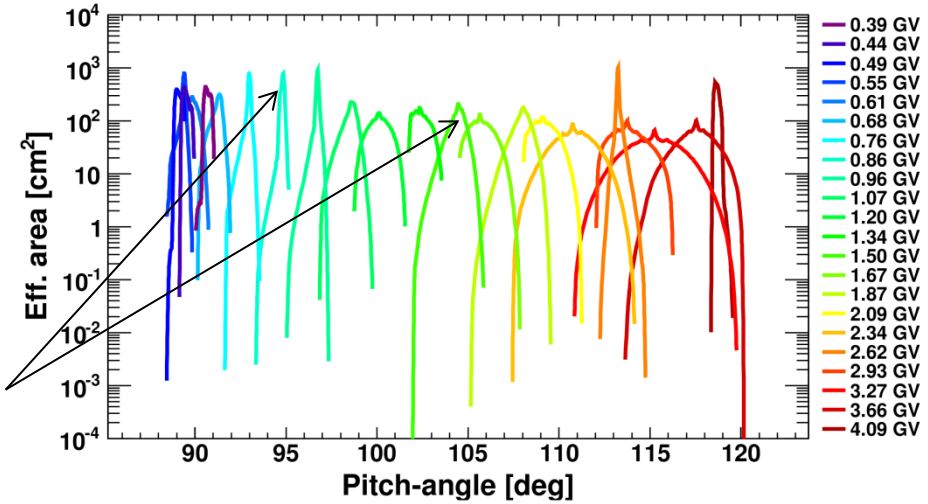

PAMELA effective area for 22 rigidity values (color code), at sample orbital position

Bruno et al., PoS(ICRC2015)085

The 2012 May 17 event
Effective area calculation

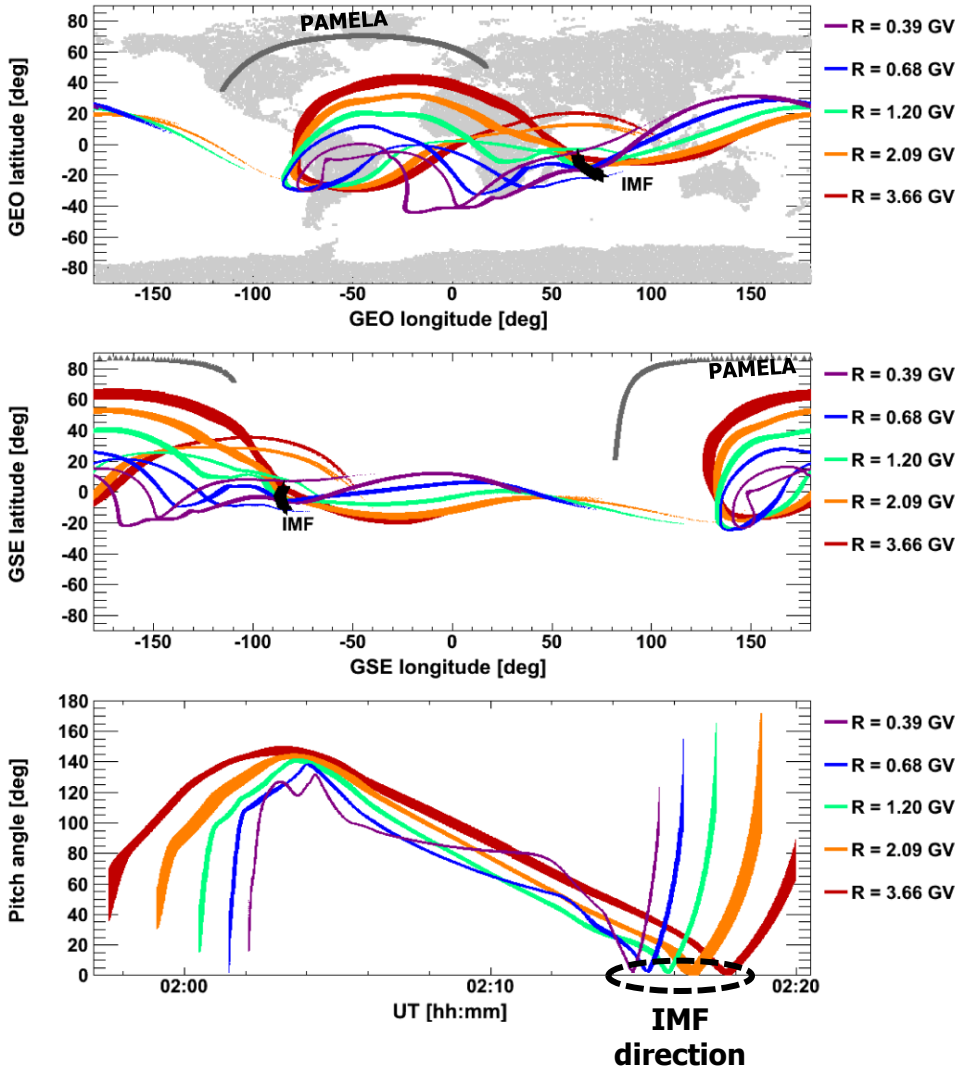

- **Asymptotic cones of acceptance** evaluated for the first PAMELA polar pass (01:57÷02:20 UT) during the May 17, 2012 SEP event. Results for sample rigidity values are shown as a function of GEO (**top panel**) and GSE (**middle panel**) coordinates;
- The pitch-angle coverage as a function of the orbital position is displayed in the **bottom panel**.
- ❖ During the satellite polar pass the asymptotic cones move in a clockwise direction and a large pitch-angle interval is covered (0÷145 deg).
- ✓ In particular, PAMELA is looking at the IMF direction between 02:14 and 02:18 UT, depending on the proton rigidity.

Fluxes are averaged over single polar passes (~22 min)

Bruno et al., PoS(ICRC2015)085

The 2012 May 17 event
Pitch-angle distribution

PAMELA vs NMs
averaged over the solar pass (01:58 - 02:20 UT)

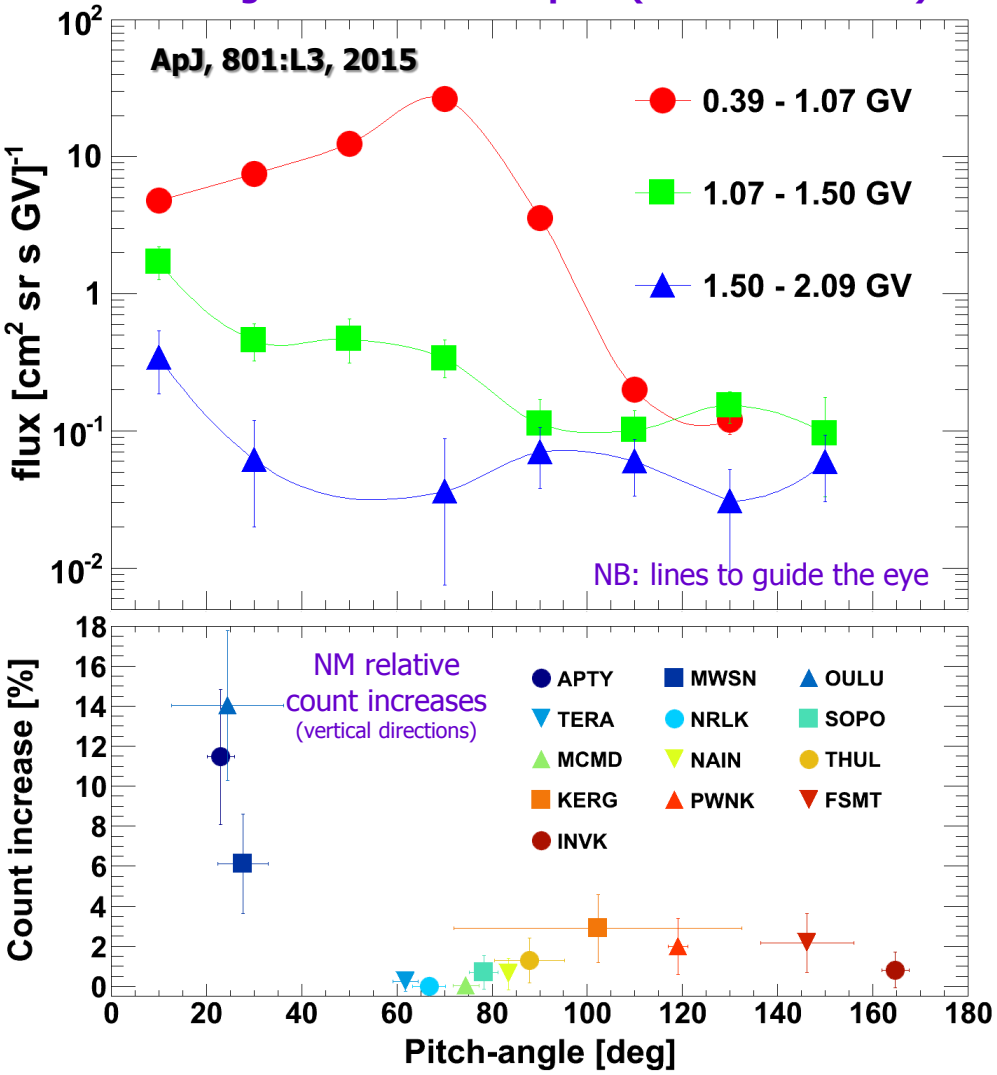

PAMELA observes two populations simultaneously with very different pitch angle distributions:

- a low-energy component (<1 GV)
  - confined to pitch angles <90°
  - and exhibiting signicant scattering or redistribution;
- and a high-energy component (>1.5 GV)
  - beamed with pitch angles <30°,
  - consistent with NM observations.
- The component with intermediate energies (1 - 1.5 GV) suggests a transition between the low and high energies.

At rigidities >1 GV, corresponding to NM data, the particles are mostly field aligned.

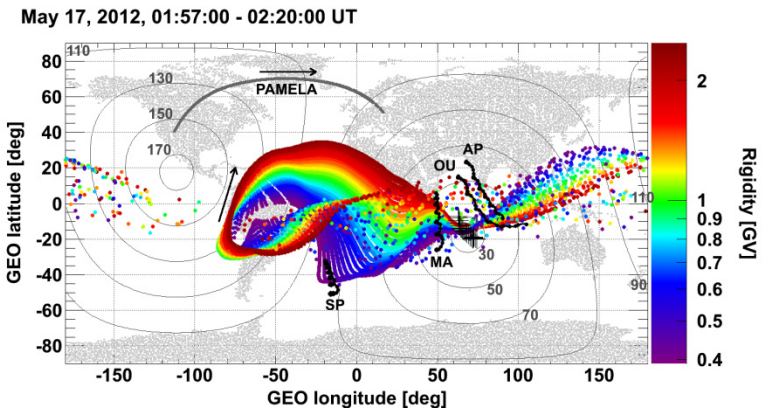

Adriani et al., 2015, ApJL, 801:L3

The 2012 May 17 event

Pitch-angle distribution

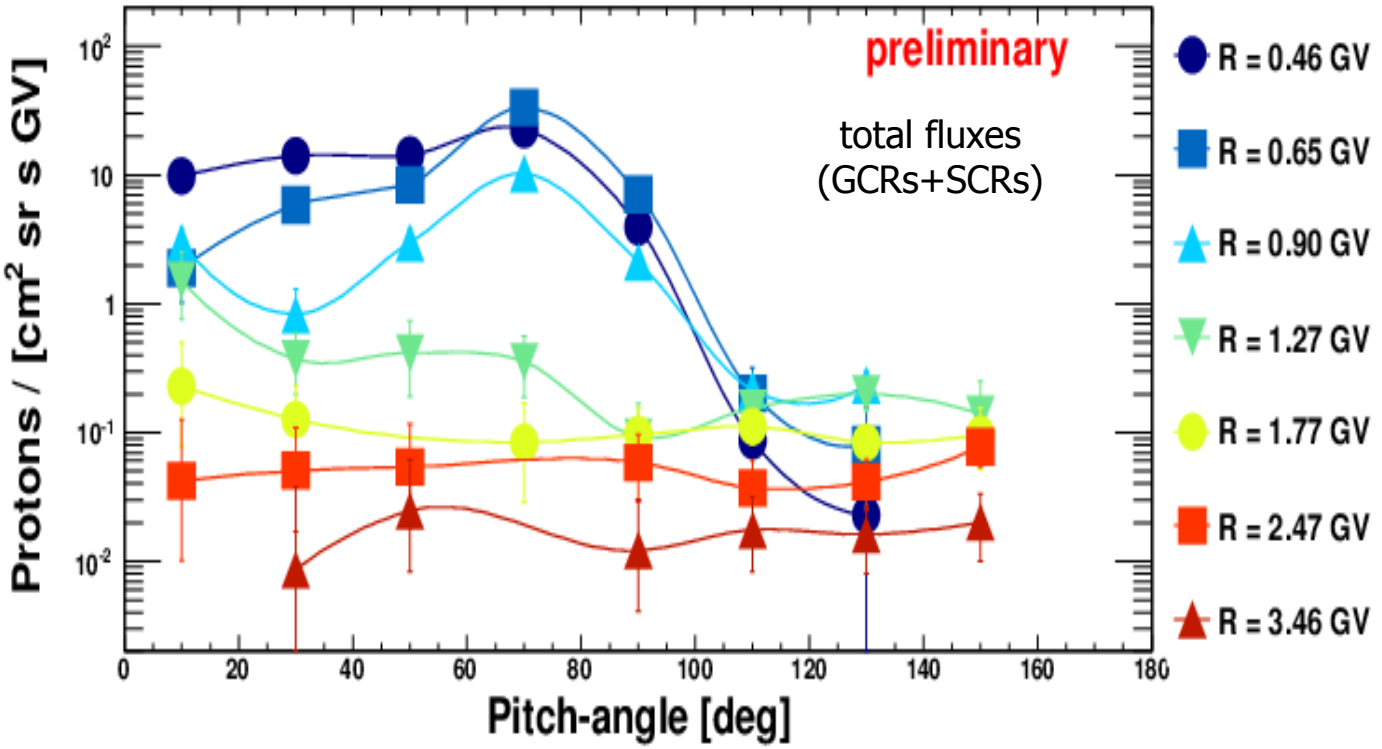

The 2012 May 17 event

Pitch-angle distributions in time

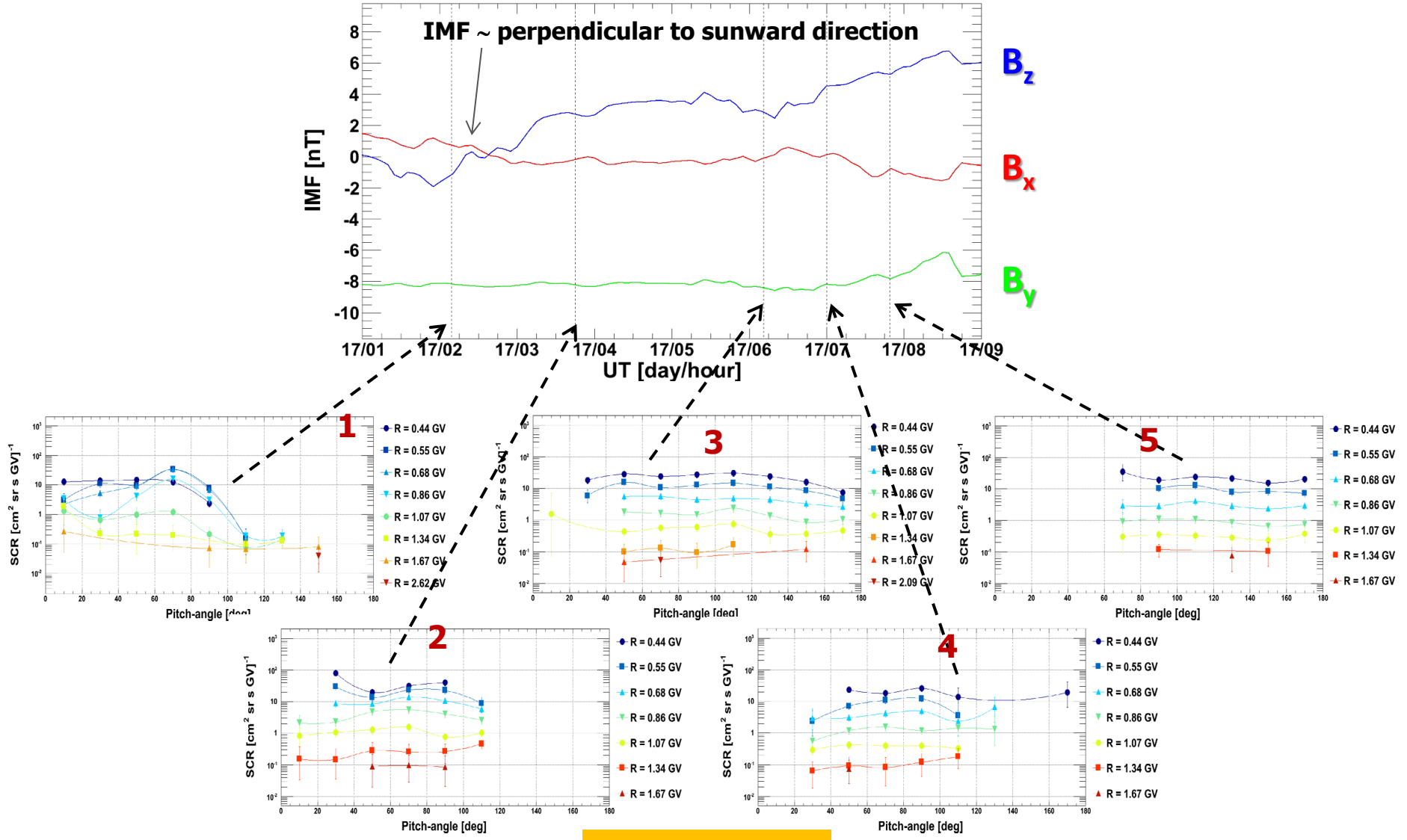

preliminary!

Conclusions

- PAMELA results improve the description of the **geomagnetically trapped** proton radiation at low altitudes (down to L~1.1 R_E) and at high energies (up to E~4 GeV), where current models suffer from large uncertainties.
  - the analysis of trapped e+/e- is in progress
  - we plan to develop a PAMELA trapped model
- PAMELA measurements provide important information on trapping and interaction processes in the geomagnetic field, and also enhance the description of **re-entrant albedo** protons (quasi-trapped, precipitating, pseudo-trapped) in different regions of the magnetosphere, including the penumbral regions.
- PAMELA data have been exploited to perform a measurement of the **geomagnetic cutoff** variations during the long lasting SEP events of 2006 December 13 and 14.
- PAMELA is providing accurate **SEP** measurements in a wide energy range
  - Its unique observational capabilities include the possibility of measuring the flux angular distribution and thus investigating possible SEP anisotropies.
  - The trajectory analysis will prove to be a vital ingredient for the interpretation of solar events observed by PAMELA during solar cycles 23 and 24.